Article

Regulation of Arsenic Mobility on Basaltic Glass Surfaces by Speciation and pH

Bergur Sigfusson, Andrew A. Meharg, and Sigurdur R. Gislason

Environ. Sci. Technol., **2008**, 42 (23), 8816-8821• DOI: 10.1021/es8001458 • Publication Date (Web): 30 October 2008

Regulation of Arsenic Mobility on Basaltic Glass Surfaces by Speciation and pH

BERGUR SIGFUSSON,*,†,‡
ANDREW A. MEHARG,† AND
SIGURDUR R. GISLASON‡
School of Biological Sciences, University of Aberdeen, AB243UU, Aberdeen, U.K., and Institute of Earth Sciences, University of Iceland, 101 Reykjavik, Iceland

Received January 15, 2008. Revised manuscript received July 22, 2008. Accepted August 21, 2008.

The importance of geothermal energy as a source for electricity generation and district heating has increased over recent decades. Arsenic can be a significant constituent of the geothermal fluids pumped to the surface during power generation. Dissolved As exists in different oxidation states, mainly as As(III) and As(V), and the charge of individual species varies with pH. Basaltic glass is one of the most important rock types in many high-temperature geothermal fields. Static batch and dynamic column experiments were combined to generate and validate sorption coefficients for As(III) and As(V) in contact with basaltic glass at pH 3−10. Validation was carried out by two empirical kinetic models and a surface complexation model (SCM). The SCM provided a better fit to the experimental column data than kinetic models at high pH values. However, in certain circumstances, an adequate estimation of As transport in the column could not be attained without incorporation of kinetic reactions. The varying mobility with pH was due to the combined effects of the variable charge of the basaltic glass with the pH point of zero charge at 6.8 and the individual As species as pH shifted, respectively. The mobility of As(III) decreased with increasing pH. The opposite was true for As(V), being nearly immobile at pH 3 to being highly mobile at pH 10. Incorporation of appropriate sorption constants, based on the measured pH and Eh of geothermal fluids, into regional groundwater-flow models should allow prediction of the As(III) and As(V) transport from geothermal systems to adjacent drinking water sources and ecosystems.

Introduction

Arsenic is released from soil and geothermal environments into ground waters through natural processes and anthropogenic activities (*1*−*3*). There are many pathways for As to threaten human health via polluted ground- or surface-waters (*2, 4*). Speciation of As is the most important factor controlling its toxicity, bioavailability, and mobility, depending mainly on the environmental parameters such as pH and redox potential (*2*). Arsenic is mostly present in aqueous environments in +III and +V oxidation states as arsenite and arsenate oxyanions and their hydrolysis species, respectively (Figure 1) (*2, 5*) with minor amounts of methyl and dimethyl As compounds being detected in some systems (*6*). As(V) forms the negatively charged oxyanions $H_2AsO_4^-$ and $HAsO_4^{-2}$ at pH values above 2 and 7, respectively, whereas As (III) forms the uncharged oxyanion H_3AsO_3 at a pH up to around 9 ($pK_a = 9.2$) (*7*). Recently the importance of thioarsenates in sulfidic geothermal waters has been reported as it has been found to be as high as 83% dissolved As under alkaline conditions (*8*).

The aqueous redox reactions of As are slow without some form of catalyst (*9*). Oxidation of As(III) is frequently facilitated by reduction of Fe(III), and the reduction of As(V) is facilitated by oxidation of sulfides (*10*) with redox processes accelerated by up to 5 orders of magnitude in geothermal waters by microbial activity (*11*). Knowledge of the kinetics of redox reactions between the individual As species can therefore play an important role when quantifying sorption processes and As transfer. The variable charges of the As species and the interacting surfaces lead to variable adsorption and retention of the respective species relative to groundwater flow. Accurate determination of the speciation of As in natural water is therefore fundamental to predict its transport in the environment.

Continental flood basalts cover an important fraction of the terrestrial surface (*12*). Arsenic concentration in terrestrial basaltic rocks ranges from 0.18 to 113 mg kg^{-1}, with an average concentration of 2.3 mg kg^{-1} (*2*). Examples include the Columbian river basalts in the U.S., the Deccan traps in India, and the Siberian traps in Russia. Furthermore, the ocean floor is primarily composed of basalt (*13*). Geothermal activity is frequently associated with basalt that can either be glassy or crystalline in volcanic terrains (*14*). Knowledge of As movement in basaltic environments, therefore, plays a key role in quantifying the global As cycle. Since Iceland is mainly composed of basaltic rocks where active seafloor spreading coincides with the occurrence of upwelling mantle plume resulting in intense volcanism (*15*), it constitutes a prime study area for understanding the role and movement of As in the environment. This geological situation leads to the widespread occurrence of high-temperature geothermal systems, some of which are currently utilized for power generation (*16*). Hydrothermal fluids, often As enriched (*17*), are pumped to the surface, where heat is extracted and electricity generated before these fluids are either pumped back into the crust through boreholes or released to adjacent surroundings. The subsequent fate of arsenic in geothermal waters raised to the surface is not fully known and there is concern that arsenic may be mobile in groundwater systems where basalt and basaltic glass are the main rock constituents (*18*).

The surface sites of basaltic glass can be considered as >SOH (where >S signifies any −OH binding atom at the surface site) that can either accept proton represented by the reaction:

$$>SOH + H^+aq = >SOH_2^+ \quad (1)$$

associated with the equilibrium constant $K_{S,1}$ or donate proton to the solution represented by the reaction

$$>SOH = SO^- + H^+aq \quad (2)$$

associated with the equilibrium constant $K_{S,2}$. The equilibrium constants $K_{S,1}$ and $K_{S,2}$ differ between the respective surface sites and consequently the point of zero charge of the surface site mixture. The chemical composition of the basaltic glass is primarily Si with lesser amounts of Al and Fe on a molar basis with Si and Al, and to a lesser extent Fe(III), as the network forming elements, and with Fe(II) occupying the

* Corresponding author e-mail: Bergur@raunvis.hi.is.
† University of Aberdeen.
‡ University of Iceland.

10.1021/es8001458 CCC: $40.75

Published on Web 10/31/2008

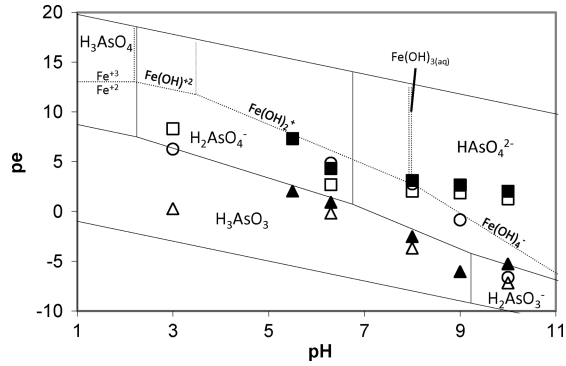

FIGURE 1. Thermodynamic system of As oxyanion species in water (7). Superimposed are Fe species with $Fe(OH)_3$(s) undersaturated. The As species have anticipated increased mobility in basaltic glass media in the following order: $H_2AsO_4^-$ < H_3AsO_4 ≈ H_3AsO_3 < $H_2AsO_3^-$ < $HAsO_4^{2-}$. Open symbols represent conditions in column experiments, closed symbols represent batch experiments. Squares represent measured pe, circles are pe calculated from Fe(II)/Fe(III) redox couple, and triangles are pe calculated from As(III)/As(V) redox couple.

space within the network (*19*). Therefore, the surface may be assumed to consist primarily of silanol sites followed by aluminol sites and to a lesser extent amorphous Fe(III) hydroxide sites.

Mobility of key As species in thermodynamic equilibrium in groundwater conditions in contact with basaltic glass with a point of zero charge at pH 6.8 (*20*) can be predicted by studying Figure 1 (*7*). Under reduced conditions the main As(III) species has −1 charge above 9.2 and is, therefore, repelled from the surface. Below pH 9.2 the species is uncharged and should, therefore, have some degree of mobility. At oxidized conditions at pH levels below 2, the dominant As(V) species is uncharged and should have high mobility. Between pH 2 and 6.8 the charges of the main species and surface sites are opposite and As(V) should be immobile at pH 3, but increasingly mobile as the pH rises and the positive charge on the surface is decreased. Above pH 6.8 the dominant As(V) species is −2 charged and is, therefore, repelled from the surface sites.

Adsorption of As(III) was predicted to be small on am-SiO_2 (*21*). Increased adsorption of As(III) on surface sites of illite, ferrihydrite, goethite, and am-$Al(OH)_3$, respectively, was observed from pH 4 to 9; however, adsorption declined on ferrihydrite, goethite, am-$Al(OH)_3$ above pH 9 (*22*−*25*) a finding that corresponds closely to the first pK_a (9.2) of H_3AsO_3. Adsorption of As(V) was predicted to be small on am-SiO_2 (*21*). Arsenic(V) was decreasingly sorbed on ferrihydrite (*23*) and am-$Al(OH)_3$ (*25*) as pH increased from 3 to 10.

The goal of this study was to predict the transfer of As oxyanions through basaltic glass media, a significant constituent of aquifers in geothermal areas and continental flood basalt areas. The main objectives were to (i) determine the rate and extent of As(III) and As(V) adsorption on the basaltic glass surface at pH 3−10, and (ii) predict whether and how As(III) and As(V) will move from high-temperature geothermal waters into shallow groundwater environments.

Experimental Section

Materials and Chemicals. The chemical reagents used in this study were of reagent grade. The reagents $NaAsO_2$, $Na_2HAsO_4.7H_20$, NaOH, and $Na_3C_6H_5O_7$ (Trisodium citrate) were obtained from BDH Chemicals. Ascorbic acid, and KI were obtained from Acros organics. $NaBH_4$ and $C_{37}H_{34}Na_2N_2O_9S_3$ (Acid Blue 9) were obtained from Sigma Aldrich Chemical Co.

The basaltic glass used in experiments was obtained from the volcanic ash of Stapafell mountain, southwestern Iceland (*19*). Preparation of the glass was carried out according to ref *25* except that the 125−250 μm size fraction was used in the current contribution. The specific surface area (1.533 m^2 g^{-1}) of the glass was measured by the three-point BET method using Kr gas.

Test Solutions. Initial column and batch experiments solutions were adjusted to pH values of 3, 6.3, 8, 9, and 10 and ionic strength of 10 mM by varying concentrations of HCl, NH_4Cl, and NH_4OH (*19*) (Supporting Information (SI) Table S1). These solutions were purged for two hours with grade 5.0 N_2 gas (BOC gases, Aberdeen), and all batch experiments were prepared and carried out in a N_2 filled glovebox. Detailed description of the experimental procedures can be found in the Supporting Information.

Batch Kinetic/Equilibrium Experiments. Stock As solutions (60 mg L^{-1}) were prepared by weighing $NaAsO_2$ and $Na_2HAsO_4.7H_2O$ daily into a 0.5 L volumetric flask and dissolved in DDI water for As(III) and As(V) solutions, respectively.

For kinetic experiments, 20 mL of 4 μM As(III) and As(V) solutions of desired pH were dispensed into 50 mL centrifuge bottles containing 2 g of basaltic glass. The samples were then shaken at 170 rpm at 30 °C (±0.1 °C) for 24, 8, 4, 1.5, 0.67, 0.2, and 0.1 h on an incubated shaker (MaxQ mini, Barnstead International).

For isotherm experiments, solutions of desired pH with As concentrations of 0.667, 1.33, 4.00, 8.01, and 16.0 μmol L^{-1}, respectively, were dispensed into 50 mL centrifuge bottles containing 2 g of basaltic glass. The samples were shaken at 170 rpm at 30 °C (±0.1 °C) for 24 h. All solutions were analyzed for As(III) by an optimized HG-AAS method (*26*) for FIA-HG-AAS and total As with FIA-HG-AAS. The As(III) method was cross validated on randomly selected samples with HPLC-ICP-MS (*27*) and the As(III)/As(V) speciation results concurred between the two techniques (SI Table S2). All As analyses were compared against the SLRS-4 Certified Reference Material. All experiments were carried out in triplicate.

Column Experiments. Basaltic glass (16 g) was packed into a 16 cm long, 1 cm i.d. PTFE column providing a porosity of 0.45 (SI Figure S2). An As containing solution was prepared by pipetting 5 mL of 60 mg/L stock solution into a volumetric flask, adding 20 mg of Acid Blue 9 that acted as a conservative tracer (*28*) into a 0.5 L volumetric flask, and filling to the mark with a solution of desired pH. Nitrogen gas was purged through the inlet solutions for two hours before pumping them onto the column. A peristaltic pump (Cole-Parmer Masterflex) pumped 1000 PV of inlet solution at 1 mL min^{-1} into the base of the column. During this period, chemical composition, pH, and Eh were monitored At stable outlet pH conditions of 3.0, 6.4, 8.1, 9.1, and 9.5(±0.1) for the initial pH 3, 6.3, 8, 9, and 10 values, respectively, four pore volumes of As containing the inlet solution were injected into the column. Finally, the column was eluted with 25 pore volumes of As-free inlet solution. A detailed description of the measurement procedure of the outlet solutions may be found in the Supporting Information. The low amount of sulfate (<0.6 μg L^{-1}) and absence of sulfide in the outlet solutions due to the low concentration of sulfur (S) in the basaltic glass ensured a minimum effect of As−S species during the experimental procedure.

Results and Discussion

Redox State of Experiments. The discrepancy between the measured pe with a platinum electrode and the calculated pe from measured redox couples As(III)/As(V) and Fe(II)/Fe(III) indicated a lack of system redox equilibrium, which has been attributed to the slow conversion between the two oxidation states (*9*). Arsenic(V) as the initial species in the

experiments, was never reduced to As(III). In the batch experiments, As(III) was partially oxidized to As(V) and nearly reached equilibrium at pH 10 (Figure 1, SI Table S4). In the column experiments, As(III) was not oxidized (Figure 1) and the Fe redox couple indicated the dominance of Fe(II) oxidation to $Fe^{III}(OH)_2^+$(aq), $Fe^{III}(OH)_3$ (aq), $Fe^{III}(OH)_4^-$ except at pH 3 and 10 where Fe^{2+} was the dominant species.

Batch Adsorption Experiments. In the batch experiments, the pH increased within hours from pH 3 to 5.5. Batch experiments carried out at an initial pH 3 value will therefore be referred to as pH 5.5 from this point on and cannot be used to predict As transport in columns at pH 3. The pH shift could have been the result of initial fast basaltic glass dissolution at pH 3 (*29*), leading to increased pH and subsequent formation of am-Al and am-Fe(III) hydroxides that would adsorb the As(III) in solution at pH 5.5 and generate the discrepancy between experimental and modeled results at pH 3 (5.5). The column experiments, however, were carried out at pH 3.0 due to the pre-experimental extended flushing period that was characterized by an initial fast rise to pH 6, which was then followed by a stepwise drop in pH values to pH 3.0 with the surface Si:Al:Fe chemical composition not differing from the fresh basaltic glass (SI Table S3 and Figure S3).

The kinetics of adsorption were analyzed according to the second order kinetic model (*30*) and a dynamic Langmuir kinetic model (*31*). The pseudo second order model was represented as follows:

$$\frac{dq_t}{dt} = k(q_e - q_t)^2 \quad (3)$$

where t is time, k is the rate constant of sorption (kg sec mol^{-1}), q_e is the amount of soluted As adsorbed at equilibrium (mol kg^{-1}), and q_t is the amount of As sorbed on the surface at any given time (mol kg^{-1}). Derivation of the second order kinetic constants may be found in the Supporting Information.

The dynamic Langmuir kinetic model was represented as

$$\frac{dq}{dt} = k_a(C_0 - q_m\Theta)(1 - \Theta) - k_d\Theta \quad (7)$$

where k_a is the first order constant for adsorption, C_0 is the initial solute concentration (mol L^{-1}), q_m is the maximum amount of adsorbate (mol kg^{-1}) (derived from experimental data described in the following As(III) section), θ is the fraction of covered surface and k_d is the first order rate constant for desorption. The kinetic Langmuir constants were derived by a method described in the Supporting Information. The constants from kinetic experiments are tabulated in SI Table S5. The pseudosecond-order model showed better fit to the data than the dynamic Langmuir model (Figures 2a and b). The Langmuir model could not simulate the fast initial sorption rate; hence, the deviation from the initial data points in Figures 2 a and b. This deviation was also evident for the pseudo second order model when the rate constant for the overall sorption (k) was used (Figures 2a and b).

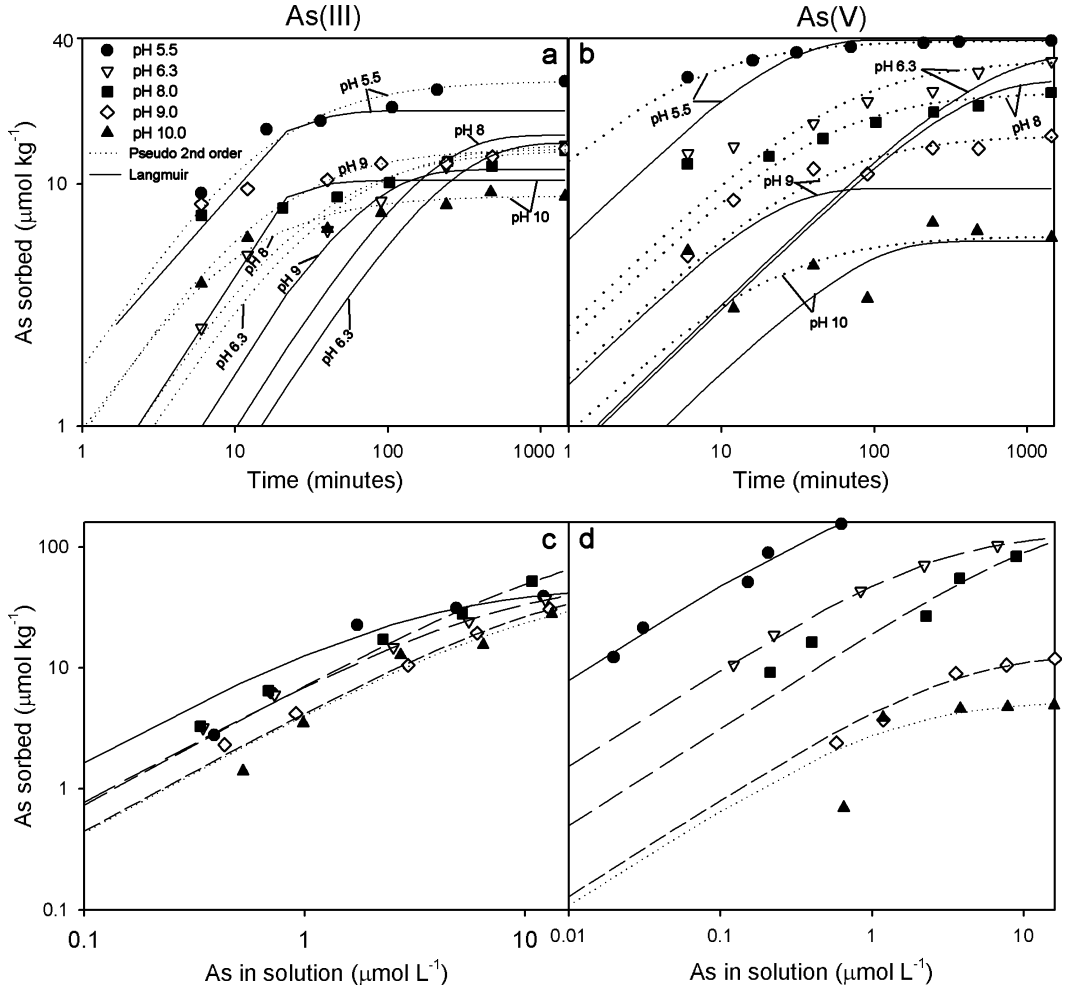

FIGURE 2. Kinetic adsorption experiments of four μmol L-1 As(III) and As(V) (b) and adsorption istotherm experiments for As(III) (c) and As(V) (d) onto basaltic glass. A complete sorption was 40 μmol kg-1. Fit to the pseudosecond- order model (dotted lines) and dynamic Langmuir model (solid lines), respectively on panels a and b. Fit to Langmuir isotherm model is represented as incremented lines on panels c and d. Adsorbent dose 2 g 20 mL-1, ionic strenth 0.01 M, temperature 30 °C.

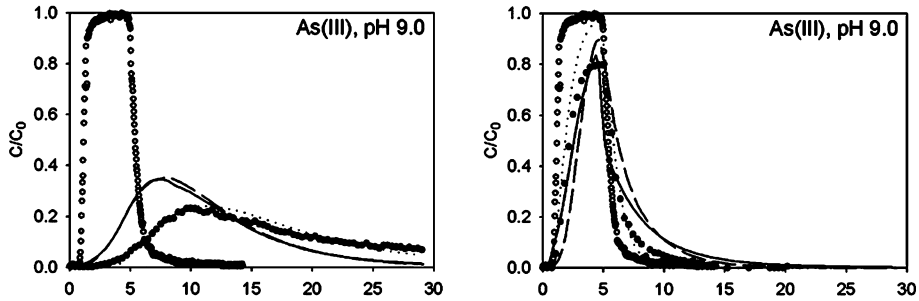

FIGURE 3. Transport of As(III) and As(V) through basaltic glass columns at pH 9. Four pore volumes of solution containing 4 μmol L-1 As and 40 mg L-1 Acid Blue 9, a conservative tracer, were injected onto column and then eluted with 25 pore volumes of As-free solution of the same pH and ionic strength. Filled circles are experimental data points, open circles are conservative tracer, hatched lines give results from pseudosecond-order, and solid lines are the dynamic Langmuir kinetic models, respectively. Dotted lines indicate the SCM model. Results from other pH values may be found in the Supporting Information.

The equilibrium adsorption isotherm data at varying pH were analyzed using the Langmuir adsorption expression:

$$q_e = \frac{q_m K_L Ce}{1 + K_L C_t} \quad (8)$$

where q_e (mol kg^{-1}) is the amount of adsorbed As at equilibrium, q_m (mol kg^{-1}) is the maximum adsorption capacity corresponding to complete monolayer coverage, C_e (mol L^{-1}) is the equilibrium solute (As) concentration, K_L is the Langmuir constant related to the energy of sorption (L mol^{-1}), and C_t is As concentration As in solution at time t. The Langmuir parameters were obtained by nonlinear least-squares regression analysis on experimental data using Excel (Microsoft) (Figures 2c and d) and are summarized in SI Table S5.

The equilibrium adsorption data were further analyzed with the generalized two layer model (*32*) incorporated into PHREEQC-2 (*33*). The surface in the surface complexation model (SCM) was considered to be a mechanical mixture of silanol, aluminol, and amorphous Fe sites (*34*) in ratios equivalent to the Si, Al, and Fe(III) ratios of the basaltic glass and surface site density as 1 μmol g^{-1} (SI Table S6). With this methodology, $\log_{ks,1}$, $\log_{ks,2}$ (5.56, −7.89, respectively) from eqs 1 and 2 were calculated based on a consistent database for a triple layer model (*21*, *34*) The intrinsic equilibrium constants for H_3AsO_3 and H_3AsO_4 adsorption reactions were estimated from isotherm experiments by iteratively optimizing experimental curves to the SCM by minimizing the differences between calculated and experimental adsorption data. Two surface reactions were assigned for As(III), formation of the bidentate inner sphere complex and the monodentate outer sphere complex (*35*) and two bidentate inner sphere complexes and one monodentate inner sphere complex for As(V) (*36*). By using the SCM, the effect of varying Cl^- concentrations in the solution could be estimated and incorporated into the model (SI Table S6), and competitive sorption was diminishing except at pH 3 where a Cl−surface complexes formed.

As(III). For all pH treatments (except pH 6.3 treatment), sorption sites were saturated with As(III) within 8 h with less than 40% As(III) sorption (Figure 2a). The initial sorption rate for As(III) was fastest at pH 5.5 (28 nmol sec^{-1} kg^{-1}) and slowest at pH 6.3 and 8 (5 and 6 nmol sec^{-1} kg^{-1}, respectively), but then increased again toward pH 10 (15 nmol sec^{-1} kg^{-1}) SI Table S5, Figure 2a). The minimum and maximum equilibrium adsorption of As(III) was calculated as 49.3 and 145 μmol kg^{-1} at pH 5.5 and pH 8, respectively, by the Langmuir isotherm (SI Table S5). The small difference detected in the maximum adsorption capacity of As(III) between pH treatments was due to the charge of the As(III) species. The As(III) occurred mainly as H_3AsO_3 up to pH 8, but as $H_2AsO_3^-$ with a percentage of 37 and 85% of the As(III) at pH 9 and 10, respectively (SI Table S4). Furthermore, a stronger negative surface charge of the glass at pH 10 explained the lower adsorption than at pH 9 (Figures 1and 2, SI Tables S4 and S5). The SCM predicted batch adsorption well over the whole pH range (Figure 2c and d). Chloride competed with As(III) below pH 6.3, and as a consequence, As(III) had limited sorption on the basaltic glass surface. The predicted increased deviation from the batch experimental data at low pH resulted in an enhanced fit to the experimental column data as will be discussed below.

As(V). Sorption sites were saturated with As(V) within 8 h at pH 5.5, 9, and 10, whereas, adsorption was not completed at the end of experiment at pH 6.3 and 8 (Figure 2b). The initial sorption rate was highest (99 nmol sec^{-1} kg^{-1}) for As(V) at pH 5.5 but lowered toward 1.3 nmol sec^{-1} kg^{-1} at pH 10 (Figure 2b, SI Table S5). The minimum and maximum equilibrium adsorption of As(V) was calculated as 442 and 2.33 μmol kg^{-1} at pH 5.5 and 10, respectively, by the Langmuir isotherm (SI Table S5).The predominant As(V) species at pH 5.5 was $H_2AsO_4^-$ which was strongly attracted to the high positive surface charge of the glass (Figure 1,SI Table S4). As the pH increased, the surface charge decreased and was close to zero at pH 6.3 and 8, resulting in a small difference in the maximum calculated adsorbance of As(V). The surface charge of the glass was increasingly negative at pH 9, resulting in a low adsorbance potential of negatively charged $HAsO_4^{2-}$ species (SI Table S4). Very limited adsorption was measured (Figure 2d) and calculated (SI Table S5) at pH 10 due to the strong repulsion of the $HAsO_4^{2-}$ from the negatively charged surface (Figure 2, SI Table S4).

Arsenic Transfer through Columns. Movement of As through experimental columns was modeled by the geochemical program PHREEQC-2 (*33*) by (i) combining the pseudosecond order kinetic model (eq 3) with the Langmuir isotherm equation (eq 8). The combination of eqs 3 and 8 was necessary since the sorption rate depends on the equilibrium sorption concentration (q_e in eq 3), which in turn depends on the As solution concentration (C_t in eq 8). Substituting eq 8 for q_e in eq 3, therefore, gives

$$\frac{dq_t}{dt} = k\left(\left(\frac{q_m K_L C_t}{1 + K_L C_t}\right) - q_t\right)^2 \quad (9)$$

Modeling was further carried out by using (ii) the dynamic Langmuir kinetic model (eq 7), and finally (iii) by surface complexation modeling (SCM). The models generated were then validated by a series of column experiments where the inlet solution contained the respective As species at 4 μmol L^{-1} along with a conservative tracer (Figure 3 and SI Figure S4). Recovery of As at the outlet of columns was estimated by integrating the area under the elution curves in Figure 3 and SI Figure S4. In the column experiments, As species were always retarded compared to the conservative tracer except

for As(V) at pH 10 (Figure 2). The experimental data were successfully modeled by kinetic approaches in 7 out of 10 systems with either kinetic models, but there was considerable discrepancy for As(III) at pH 3 (due to the pH shift to 5.5) and 6.3 and for As(V) at pH 8 (SI Figure S4). The SCM modeled high pH experimental conditions successfully (Figure 3 and SI Figure S4), indicating that the dominant reactions reached equilibrium sufficiently quickly as the SCM used was an equilibrium-based model. For As(III) inadequate fit by the SCM at pH 6.3−8 and for as As(V) at pH 8 was due to slow surface reactions that did not reach equilibrium in the column which is in agreement with As(V) adsorption rates onto aluminum oxide (*37*).

As(III). The maximum adsorption of As(III), as with many oxyanions, occurs around its first pK_a (pH 9.2) on surfaces such as ferrihydrite (pH 8−10 (*23*),), am-Al$(OH)_3$ (pH 7−9 (*25*),) and coprecipated Al:Fe hydroxides (pH 8−9 (*38*),). At pH 9 and 10, 90% of As(III) was recovered from the outlet of the column, and less than 2% of the available surface sites (q_m) in the column were occupied with As after elution (SI Table S7). Both kinetic models provided excellent fit for As(III) at pH 10 but a slightly weaker fit at pH 9 (Figure 3 and SI Figure S4). At pH 8, the dynamic Langmuir model simulated data well but a less strong fit was generated by the pseudosecond-order model. At pH 8, 68% of the injected As(III) was recovered from the column's surface sites, which were 2% occupied (SI Table S7.) All As(III) was recovered from the pH 3 experiment, though least from the pH 8 (68%) experiment where the available surface sites for sorption (q_m = 145 μmol kg^{-1}) of As(III) were most abundant. However, As(III) showed the highest retardation at pH 9 followed by 10, then 8 ≈ 6.3, and at pH 3, the retardation was limited, results are in agreement with the fastest initial adsorption rates measured at pH 9 and 10 (Figure 3 and SI Figure S4 and Table S5). At pH 10 the solubility of am-Al$(OH)_3$ and Fe(III)-hydroxides are higher than at pH 6−9 (*39*), allowing more fluctuations in pH and solute concentrations before the hydroxides start precipitating. The shift from pH 3 to 5.5 in batch experiments may have led to a a formation of am-Al and am-Fe(III) hydroxides that would adsorb the As(III) in solution at pH 5.5 and generate the discrepancy between the experimental and modeled results at pH 3 (5.5). The SCM did not allow for surface precipitation and assumed constant ratio of different sorption sites at different pH levels (Figure S3 and SI Table S3) and modeled the As(III) sorption at pH 3 sufficiently when the chloride sorption reaction was taken into account (SI Figure S4).

As(V). All measured and modeled data for As(V) showed consistently similar trends from slow and incomplete sorption at pH 10 to fast and extensive sorption at pH 3 (Figures 1, 2, and 3, and SI Table S5). At pH 9 and 10, 95% of As(V) was recovered from the outlet of the column and 11.8 and 38.6% of available surface sites (q_m) were occupied by As after elution, respectively (SI Table S7). The adsorption rates (h, k, and ka) and capacity (q_m) were smallest at these pH levels (SI Table S5). Both kinetic models successfully described column experimental data at pH 9 and 10 (Figure 3 and SI Figure S4). At pH 8 neither kinetic models described the column data successfully (SI Figure S4) where 55% of As(V) was recovered while occupying less than 2% of the columns adsorption capacity (q_m = 145 μmol kg^{-1}) (SI Tables S5 and S7). Both kinetic models described experimental data for As(V) well at pH 3 and 6.3. The difference in pH at 5.5 in the batch experiments and pH 3 in the column experiments was not sufficient to show discrepancy between the data and the kinetic models as the basaltic glass surface sites were very far from being saturated (0.0 and 0.6%) and almost no As(V) (1 and 1%) was recovered from the column outlets at pH 3 or 6.3, respectively (SI Table S7). On the contrary, 95% of As(V) was recovered at both pH 9 and 10 with 11.8 and 38.6% of sorption sites being occupied, respectively, indicating a large shift in sorption capacity as pH is shifted within the system.

Implication for Regional Groundwater Flow Models. During recent years, injection of spent geothermal wastewaters has received increased attention, although many geothermal power plants still release wastewater from discharging boreholes and production water at the surface or in shallow boreholes. The injection reduces declining pressures and extends the sustainability of the geothermal system (*40*). Furthermore, injection prevents the release of unwanted chemicals in elevated concentrations into the surface environment.

An important part in successful and sustainable utilization of geothermal energy lies in constructing models to predict thermal energy- and groundwater flow in the respective area. These models allow the prediction of movement of wastewater from the geothermal power plants. The current study highlights the importance of accurate definition of geochemical characteristics of the aquifers and the pollutant carrying water. An accurate prediction of As movement from geothermal power plant effluents to the surrounding environments relies on the knowledge of (i) the surface characteristics and hydraulic conductivity of the aquifer, (ii) the speciation of As in the geothermal effluent, and (iii) the ability of the aquifer and geothermal water to maintain or alter the speciation of As when it moves trough the aquifer. Arsenic in high-temperature geothermal water is primarily As(III) (*41*) or on thioarsenate forms that can transform to As(III) and As(V) under atmospheric conditions (*8*). Results generated in the current contribution can be applied to wastewater discharging from boreholes and to that released into shallow groundwater and suggest that alkaline geothermal waters in basaltic environments should be maintained in a reduced condition before shallow injection to prevent oxidation of As(III) to As(V), which is very mobile under alkaline conditions (Figures 1, 2, and 3). In contrast, acid geothermal waters should be oxidized before injection into the ground due to the high sorption capacity of basaltic glass for As(V) at low pH provided that the adsorption rate of As(V) is faster than the reduction rate of As(V) to As(III) and all As(V) can be removed from the solution before the pH of the system is elevated due to weathering of the aquifer rocks. For decisions regarding injection into deep aquifers at higher temperatures, further research needs to be carried out as the thermodynamic properties of arsenic species change significantly as temperature increases (*42*). Finally, further study is needed to assess the importance of thioarsenic species in sulfidic geothermal water (*8*).

Acknowledgments

Bergur Sigfusson would like to thank Rannveig Guicharnaud for valuable discussions and constructive criticism during this work. Thanks to Tony Appelo and Jón Örn Bjarnason for help in the modeling work, to Sigurdur Markus Hafsteinsson for the SEM figures and to Eric Oelkers for the BET analyses. This study was supported by the Icelandic Research Fund 050204033, Reykjavik Energy and the Icelandic Graduate Research Fund.

Supporting Information Available

Validation of the speciation analyses, figures of the experimental column setup, and coefficients generated in the current contribution. In addition, the chemical composition of all solutions and the basaltic glass surface is also provided as well as the reactions used in the SCM and their equilibrium constants. This material is available free of charge via the Internet at http://pubs.acs.org.

Literature Cited

(1) Rice, K. C.; Conko, K. M.; Hornberger, G. M. Anthropogenic sources of arsenic and copper to sediments in a suburban lake, Northern Virginia. *Environ. Sci. Technol.* **2002**, *36*, 4962–4967.

(2) Smedley, P. L.; Kinniburgh, D. G. A review of the source, behaviour and distribution of arsenic in natural waters. *Appl. Geochem.* **2002**, *17*, 517–568.

(3) Nimick, D. A.; Moore, J. N.; Dalby, C. E.; Savka, M. W. The fate of geothermal arsenic in the Madison and Missouri Rivers, Montana and Wyoming. *Water Resour. Res.* **1988**, *34*, 3051–3067.

(4) Mandal, B. K.; Suzuki, K. T. Arsenic round the world: a review. *Talanta* **2002**, *58*, 201–235.

(5) Ferguson, J. F.; Gavis, J. A. A review of the arsenic cycle in natural waters. *Water res.* **1972**, *6*, 1259–1274.

(6) Hung, D. Q.; Nekrassova, O.; Compton, R. G. Analytical methods for inorganic arsenic in water: a review. *Talanta* **2004**, *64*, 269–277.

(7) Wolery, T. J. *>EQ3/6, A Software Package for Geochemical Modeling of Aqueous Systems*; Lawrence Livermore National Laboratory: Livermore, CA, 1992.

(8) Planer-Friedrich, B.; London, J.; McCleskey, R. B.; Nordstrom, D. K.; Wallschlager, D. Thioarsenates in geothermal waters of Yellowstone national park: Determination, preservation and geochemical importance. *Environ. Sci. Technol.* **2007**, *41*, 5245–5251.

(9) Gmelin, L. Arsenic. *Gmelin-Kraut's Handbuch der anorganischen Chemie. System nummer 17*; Verlag Cemie: Weinheim, 1952.

(10) Cherry, J. A.; Shaikh, A. U.; Tallman, D. E.; Nicholson, R. V. Arsenic species as an indicator of redox conditions in groundwater. *J. Hydrol.* **1979**, *43*, 373–392.

(11) Nordstrom, D. K., Ball, J. W., McCleskey, R. B. Oxidation reactions for reduced Fe, As, and S in thermal outflows of Yellowstone National park: biotic or abiotic? In *Water rock interaction. Proceedings of the 11th International Symposium on Water-Rock Interaction, WRI-11*; Wanty, R. B., Seal R. R., Eds.; Balkema,Saratoga Springs, NY, 2004.

(12) Jerram, D. A.; Widdowson, M. The anatomy of Contintal Flood Basalt Provinces: geological constraints on the processes and products of flood volcanism. *Lithos* **2005**, *79*, 385–405.

(13) Ronov, A. B.; Yaroshevsky, A. A. New model of earths crust chemical-structure. *Geokhimiya* **1976**, *12*, 1763–1795.

(14) Mottl, M. J.; Holland, H. D. Chemical exchange during hydrothermal alteration of basalt by seawater-I. Experimental results for major and minor components of seawater. *Geochim. Cosmochim. Acta* **1978**, *42*, 1103–1115.

(15) Schilling, J. G. Iceland mantle plume—Geochemical study of Reykjanes Ridge. *Nature* **1973**, *242*, 565–571.

(16) Armannsson, H.; Fridriksson, T.; Kristjansson, B. R. CO2 emissions from geothermal power plants and natural geothermal activity in Iceland. *Geothermics* **2005**, *34*, 286–296.

(17) Wetang'ula, G. N. ; Snorrason S. S. Geothermal wastewater disposal: Chemical stress assessment Thingvallavatn—Iceland. *Proc. World Geotherm. Congr.* **2005**.

(18) Arnorsson, S. Arsenic in surface- and up to 90°C ground waters in a basalt area, N-Iceland: processes controlling its mobility. *Appl. Geochem.* **2003**, *18*, 1297–1312.

(19) Oelkers, E. H.; Gislason, S. R. The mechanism, rates and consequences of basaltic glass dissolution: I. An experimental study of the dissolution rates of basaltic glass as a function of aqueous Al, Si and oxalic acid concentration at 25(deg)C and pH = 3 and 11. *Geochim. Cosmochim. Acta* **2001**, *65*, 3671–3681.

(20) Guy, C.; Schott, J. Multisite surface reaction versus transport control during hydrolysis of a complex oxide. *Chem. Geol.* **1989**, *78*, 181–204.

(21) Sahai, N.; Sverjensky, D. A. Solvation and electrostatic model for specific electrolyte adsorption. *Geochim. Cosmochim. Acta* **1997**, *61*, 2827–2848.

(22) Manning, B. A.; Goldberg, S. Adsorption and stability of arsenic(III) at the clay mineral-water interface. *Environ. Sci. Technol.* **1997**, *31*, 2005–2011.

(23) Raven, K. P.; Jain, A.; Loeppert, R. H. Arsenite and arsenate adsorption on ferrihydrite: Kinetics, equilibrium and adsorption envelopes. *Environ. Sci. Technol.* **1998**, *32*, 344–349.

(24) Manning, B. A.; Fendorf, S. E.; Goldberg, S. Surface structures and stability of arsenic(III) on goethite: Spectroscopic evidence for inner-sphere complexes. *Environ. Sci. Technol.* **1998**, *32*, 2383–2388.

(25) Arai, Y.; Elzinga, E. J.; Sparks, D. L. X-ray adsorption spectroscopic investigation of arsenite and arsenate adsorption at the aluminum oxide-water interface. *J. Colloid Interface Sci.* **2001**, *235*, 80–88.

(26) Masscheleyn, P. H.; Delaune, R. D.; Patrick, W. H. A. Hydride generation atomic-absorption technique for arsenic speciation. *J. Environ. Qual.* **1991**, *20*, 96–100.

(27) Williams, P. N.; Price, A. H.; Raab, A.; Hossain, S. A.; Feldmann, J.; Meharg, A. A. Variation in arsenic speciation and concentration in paddy rice related to dietary exposure. *Environ. Sci. Technol.* **2005**, *39*, 5531–5540.

(28) Mon, J.; Flury, M.; Harsh, J. B. Sorption of four triarylmethane dyes in a sandy soil determined by batch and column experiments. *Geoderma* **2006**, *133*, 217–224.

(29) Gislason, S. R.; Oelkers, E. H. Mechanism, rates, and consequences of basaltic glass dissolution: II. An experimental study of the dissolution rates of basaltic glass as a function of pH and temperature. *Geochim. Cosmochim. Acta* **2003**, *67*, 3817–3832.

(30) Ho, Y. S.; McKay, G. Pseudo-second order model for sorption processes. *Process Biochem.* **1999**, *24*, 451–465.

(31) Langmuir, I. The adsorption of gases on plane surfaces of glass, mica and platinum. *J. Am. Chem. Soc.* **1918**, 1361–1403.

(32) Dzombak, D. A.; Morel, F. M. M. *Surface Complexation Modeling: Hydrous Ferric Oxide*; John Wiley & Sons:New York, 1990.

(33) Parkhurst, D. L.; Appelo, C. A. H. User'sguide to PHREEQC (Version 2)—A computer program for speciation, batch-reaction, one-dimensional transport, and inverse geochemical calculations, U. S. G. S. *Wat. Res. Invest. Report* **1999**, *9*, 9–4259.

(34) Sahai, N.; Sverjensky, D. A. Evaluation of internally consistent parameters for the triple-layer model by systematic analysis of oxide surface titration data. *Geochim. Cosmochim. Acta* **1997**, *61*, 2801–2826.

(35) Sverjensky, D. A.; Fukushi, K. A predictive model (ETLM) for As(III) adsorption and surface speciation on oxides consistent with spectroscopic data. *Geochim. Cosmochim. Acta* **2006**, *70*, 3778–3802.

(36) Fukushi, K.; Sverjensky, D. A. A predictive model (ETLM) for arsenate adsorption and surface speciation on oxides consistent with spectroscopic and theoretical molecular evidence. *Geochim. Cosmochim. Acta* **2007**, *71*, 3717–3745.

(37) Arai, Y.; Sparks, D. L. Residence time effects on arsenate surface speciation at the aluminum oxide-water interface. *Soil Sci.* **2002**, *167*, 303–314.

(38) Masue, Y.; Loeppert, R. H.; Kramer, T. A. Arsenate and arsenite adsorption and desorption behavior on coprecipated aluminium:iron hydroxides. *Environ. Sci. Technol.* **2007**, *41*, 837–842.

(39) Lindsay, W. L. *Chemical Equilibria in Soils*; John Wiley & Sons: New York, 1979.

(40) Majer, E. L.; Peterson, J. E. The impact of injection on seismicity at The Geysers, California Geothermal Field. *Int. J. Rock Mech. Mineral. Sci* **2007**, *44*, 1079–1090.

(41) Yokohama, T.; Takahashi, Y.; Tarutani, T. Simultaneous determination of arsenic and arsenious acids in geothermal water. *Chem. Geol.* **1993**, *103*, 103–111.

(42) Halter, W. E.; Pfeifer, H. R. Arsenic(V) adsorption onto alpha-Al_2O_3 between 25 and 70 degrees C. *Appl. Geochem.* **2001**, *16*, 793–802.

ES8001458